Modeling Heat and Mass Transfer in Osmotic Evaporation Process

J. Romero
Institut Européen des Membranes, UM2, 34090 Montpellier - Cedex 5, France
and
Dept. Ing. Química, Univ. Santiago de Chile, 3363 Santiago, Chile

G. M. Rios, J. Sanchez, and S. Bocquet
Institut Européen des Membranes, UM2, 34090 Montpellier - Cedex 5, France

A. Savedra
Dept. Ing. Química, Univ. Santiago de Chile, 3363, Santiago, Chile

A model for the mass- and heat-transfer phenomena in an osmotic evaporation process was developed based on the transfer of solvent from one aqueous solution to be concentrated to a second one separated by a macroporous hydrophobic membrane. The transfer is realized in vapor phase through the membrane porosity as a consequence of the gradient on water activity between both solutions. This technique has the major advantage to work at relatively low temperature and in nearly isothermal conditions, which is very useful to treat thermosensitive products such as fruits and vegetable juices, or other solutions from biotech industries. A series-resistance model for mass and heat transfer was developed considering four regions, which include the membrane layers and different boundary regions at interfaces. The high values of flow measured in a previous experimental work are compared with those obtained by simulation. In addition, the relative importance of various resistances to overall process performance is established. Basic mechanisms that help optimize membrane structural characteristics, plant design and scale-up are also discussed.

Introduction

Today, a large variety of membranes are used in numerous processes devoted to molecular-scale separation in liquids or gases. The most classic operations are ultrafiltration, electrodialysis, pervaporation, and gas separation. In the last few years new techniques that can be summarized under the name "membrane contactors" have been proposed (Kunz et al., 1996). In these processes the membrane, which is generally macroporous, acts as a barrier, preventing downstream and upstream phase mixing and allowing the transfer of some fluid components through the membrane porosity. In contrast to the phenomena occurring in classic membrane processes, there is no selectivity due to the material itself, and diffusion mechanisms generally prevail.

Osmotic evaporation (OE) is a concentration technique for aqueous mixtures based on the use of macroporous and hydrophobic membranes, typically made of PTFE or polypropylene. This technique is regarded with interest in the processing of liquid foods, for example, for the concentration of fruit and vegetable juices and other heat-sensitive products, because it has the major advantage of processing in nearly isothermal conditions. Osmotic evaporation can be used to selectively extract the water from aqueous solutions under atmospheric pressure and at ambient temperature, thus avoiding thermal degradation of the solutions (Courel et al., 2000a). In addition, the energy consumption in OE is much lower than in reverse osmosis (Kunz et al., 1996).

In the OE process the porous hydrophobic membrane separates two circulating liquid phases. Under appropriate working conditions, the membrane made of a hydrophobic polymer cannot be wetted by the liquids, thus creating vapor–liquid interfaces at each pore entrance. The force that generates the water flow through the immobile gas phase

Correspondence concerning this article should be addressed to G. M. Rios.

within the pores is a difference in activity between the feed solution (fruit juice) on one side and a hypertonic solution, typically a concentrated brine, on the opposite side. This difference in activity results in a water-vapor pressure difference between the diluted solution upstream and the concentrated brine downstream. Efforts have been made to optimize the operating conditions in order to reach competitive fluxes at an industrial scale (Lefebvre et al., 1987; Deblay, 1994).

In this process, it is commonly admitted that mass transport can be split into three steps: the initial and the final step correspond to the water transport in liquid phase through boundary layers, from the bulk of the dilute solution toward the evaporation interface and vice versa, from the condensation surface to the bulk of the brine. Models of gas diffusion in porous media, like Knudsen or molecular diffusion, have been used to describe mass transfer across the membrane (Courel et al., 2000b; Kunz et al., 1996). The application of the models requires a detailed knowledge of many parameters that describe the porous structure; but they are usually not available from commercial suppliers.

Rigorous approaches, which tend to combine mass and heat transfer, have emerged in the literature for the membrane distillation (MD) process (Godino et al., 1996; Peña et al., 1998).

In the OE process, which is theoretically isothermal if the resistance to heat transfer is negligible, there is always a thermal effect due to the evaporation–condensation phenomena through the membrane. The heat transfer through the membrane and the boundary layers that develop in the circulating solutions will integrate the temperature polarization. A first analysis of thermal effects has been proposed by Gostoli (1999), with a model of compartments at steady state. Up to now, however, no complete model able to couple simultaneously heat and mass transfer in OE, with a view of designing and optimizing the global process, has been published.

In this work, we present a new model that takes four regions in series into consideration, each associated to one specific calculation module. This model involves the resolution of nonlinear equations considering the transport phenomena and phase equilibria in a system constituted by the membrane and the boundary layers that are developed in the circulating liquid solutions.

The model allows us to estimate the water-vapor flow through the membrane, the temperatures and concentrations at interfaces, and in the boundary layers for different hydrodynamic regimes, structural, heat- and mass-transfer conditions.

This quite general model should be easily extended to other membrane-contactor operations (Bandini et al., 1997; Lawson and Lloyd, 1997; Iversen et al., 1997; Gabelman and Hwang, 1999), such as perstraction or membrane adsorption, or even membrane reactor, by slightly modifying the arrangement and/or content of the basic modules (Mulder, 1996).

Theoretical Approach

To test the basic assumptions of the model, and to then carry out the investigation of the working parameters' sensitivity, we referred systematically to the earlier data in the literature (Kunz et al., 1996) and also to the very recent results obtained by our group (Courel, 1999; Courel et al., 2000a).

The classic membranes used in this work are hydrophobic macroporous membranes formed of a polytetrafluoroethylene separative layer that is deposited on a polypropylene support. The solution to be concentrated is fed on the PTFE layer side, whereas the brine circulates along the support. As far as the mean pore size of the support being very large and the material not being very hydrophobic, it could be considered that the vapor phase just fills the PTFE layer while the brine settles into the macroporosity of the support.

Thus the model is based on four resistances in series. They correspond, respectively, to the boundary layer, which is formed in the solution to be treated at the surface of the hydrophobic porous layer, to the hydrophobic porous layer, which is filled with gas, to the macroporous support, which is filled with stagnant liquid, and to the second boundary layer which settles on the side of the extraction brine. Figure 1 shows the different layers considered for modeling purposes.

Mass transfer

To outline the mechanisms of transport through the membrane, the hydrodynamic conditions in the membrane module have been simplified. In the study of the mass transfer, we considered the solution to be treated as only pure water; thus the resistance to the mass transfer due to this boundary layer could be ignored. As explained earlier, a second assumption was made when considering the support wetted with the brine to the point where it meets the hydrophobic layer.

Two mechanisms are possible for water vapor transport through the hydrophobic layer: Knudsen and molecular diffusion. The permeance for a Knudsen regime is given by Eq. 1

$$G_{Kn} = -\frac{N_w}{\Delta p_w} = \frac{N_w}{p_{wf} - p_{wp}} = \frac{2}{3}\frac{\epsilon_{hl} r_{hl}}{\tau_{hl} L_{hl}}\left[\frac{8}{\pi RTM_w}\right]^{0.5}, \quad (1)$$

where r_{hl} is the average pore radius of the hydrophobic layer, L_{hl} is the thickness, ϵ_{hl} is the porosity, τ_{hl} is the tortuosity, and M_w is the molecular weight of the water.

In the case of molecular diffusion regime the permeance is given by

$$G_{MD} = -\frac{N_w}{\Delta p_w} = \frac{P}{RT}\frac{\epsilon_{hl}}{\tau_{hl}}\frac{D_{wa}}{L_{hl}}\frac{1}{p_{wf} - p_{wp}}\ln\left(\frac{P - p_{wp}}{P - p_{wf}}\right). \quad (2)$$

In this particular situation, D_{wa} represents the diffusion coefficient of the water vapor in the air retained within the pores.

At steady state, the water-vapor flow should be the same through all layers. If the extraction brine penetrates the structure of the membrane support, we can make the assumption that the transport mechanism through this layer is the molecular diffusion into the liquid phase contained in the macro-
porous matrix. In this case, the flow will be given by Eq. 3:

$$N_w = \frac{\rho^{\text{sup}}_{\text{brine}}}{M^{\text{sup}}_{\text{brine}}}\frac{\epsilon_s}{\tau_s}\frac{D_{w_{\text{CaCl}_2}}}{L_s}\ln\left(\frac{1 - x^s_{wp}}{1 - x^m_{wp}}\right), \quad (3)$$

where $\rho^{\text{sup}}_{\text{brine}}$ and $M^{\text{sup}}_{\text{brine}}$ are the density and the molecular weight of the brine. For calculation purposes we considered

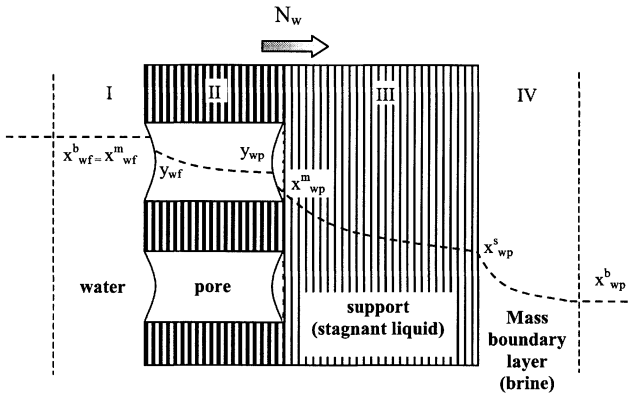

Figure 1. Mass transfer: concentration profile in the different layers of the system.

the average values of both parameters through the support layer thickness.

The last resistance, taken into account in the model is the boundary layer formed in the brine that is placed on the proximity of the support. The presence of this layer along the membrane surface can significantly affect the global mass transfer, especially at low circulation rates. The water flow through this boundary layer is given by Eq. 4:

$$N_w = k_{bl}\left(x^s_{wp} - x^b_{wp}\right). \tag{4}$$

The mass-transfer coefficient in Eq. 4 is calculated by Eq. 5, a Sherwood correlation for turbulent flow (Mulder, 1996)

$$Sh = b_1 Re^{b_2} Sc^{b_3}. \tag{5}$$

Vapor – liquid equilibrium

Estimation of the water activity in the concentrated brine is carried out using the modified ASOG group contribution method (Correa et al., 1997). The modified ASOG method is a combination of the UNIFAC method and considerations of the Debye–Hückel theory. A routine was written in Matlab language. It was introduced into the general program as a function of the brine concentration.

With this method, the water activity coefficient in the brine at the interface with the gas layer within the pores is calculated by three terms: a combinatorial term ($\ln \gamma_i^C$), which considers the shape and size of each group, a residual term ($\ln \gamma_i^R$), which considers the steric interactions between all the groups present in the solution, and a third term ($\ln \gamma_i^{D-H}$), which accounts for the effect of electrostatic interactions. If all long-range interactions of the Debye–Hückel type are considered, the three contributions have to be added, giving Eq. 6:

$$\ln \gamma_i = \ln \gamma_i^C + \ln \gamma_i^R + \ln \gamma_i^{D-H}. \tag{6}$$

In Figure 2 the estimated activity values calculated as described earlier are compared with the experimental data given by Courel (Courel, 1999). We can observe that there is good agreement between experimental and theoretical values.

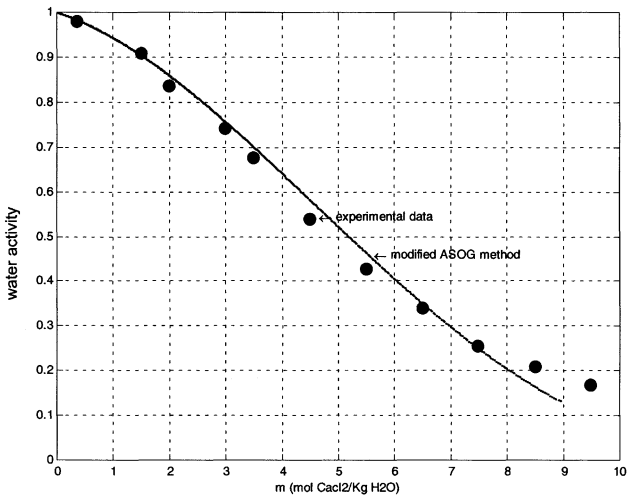

Figure 2. Water activity in a solution of $CaCl_2$ at 298 K.

Heat transfer

In the osmotic evaporation process, mass transfer is always accompanied by heat transfer, because phase changes like water evaporation and condensation occur on both sides of the hydrophobic membrane. In the experiments conducted by Courel (Courel et al., 2000a) the two fluids are maintained at the same temperature. Taking this consideration into account, we can represent the temperature polarization profile that takes place, as in Figure 3. This phenomenon could be responsible for the decrease in water-vapor flow through the membrane caused by the reduction of the process driving force, that is, the partial-pressure difference across the hydrophobic layer.

At steady state the heat flow must be the same whatever the layer of the system. From Figure 3 we can write the following equations (Gostoli, 1999)

$$Q_{\mathrm{I}} = h_f\left(T^b_f - T^m_f\right) \tag{7}$$

$$Q_{\mathrm{II}} = N_w \Delta H_v + h_{hl}\left(T^m_f - T^m_p\right) \tag{8}$$

$$Q_{\mathrm{III}} = h_s\left(T^m_p - T^s_p\right) \tag{9}$$

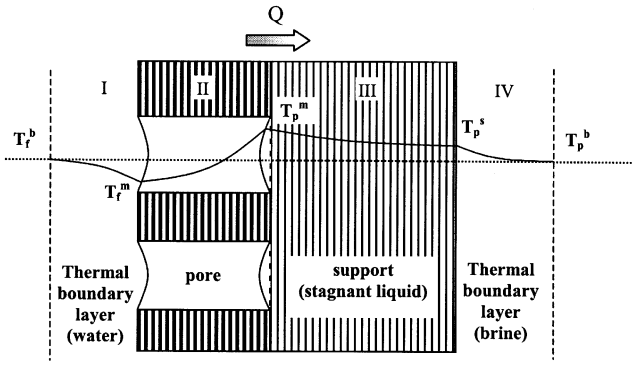

Figure 3. Thermal effects in osmotic evaporation process under stationary conditions.

$$Q_{IV} = h_{brine}\left(T_p^s - T_p^b\right) \tag{10}$$

$$Q_I = Q_{II} = Q_{III} = Q_{IV}. \tag{11}$$

The heat-transfer coefficients in the solid barrier were calculated from the thermal conductivities of the polymer and the fluid that penetrates the pores. For the hydrophobic layer, the coefficient was calculated by the following equation

$$h_{hl} = \frac{k_{hl}^T}{L_{hl}}, \tag{12}$$

where

$$k_{hl}^T = \epsilon_{hl} k_{gas}^T + (1 - \epsilon_{hl}) k_{polymer}^T, \tag{13}$$

while for the support penetrated by the liquid, Eq. 14 was used

$$h_s = \frac{k_s^T}{L_s}, \tag{14}$$

where

$$k_s^T = \epsilon_s k_{brine}^T + (1 - \epsilon_s) k_{polymer}^T. \tag{15}$$

Mathematical and numerical methods

To solve the system equations, a program was written in Matlab language (Mokhtari, 2000). In the first step, the system was considered under isothermal conditions and the model built without considering the influence of the temperature polarization. Then in the second step a more complete program was realized by coupling the mass- and heat-transfer phenomena. The Regula Falsi algorithm (Quarteroni, 2000; Kreyszig, 1991) was applied to reduce the number of iterations. In this program it is possible to modify all the operating variables, the type of mass- and heat-transfer mechanisms, and the structural parameters of the membrane.

Figure 4 contains the algorithm used to estimate the water flow through the membrane. It is constructed from several elementary cells that are associated with the different layers of the system, plus one specific cell for the introduction of structural parameters/operating conditions and other modules that generate the concentration values at interfaces.

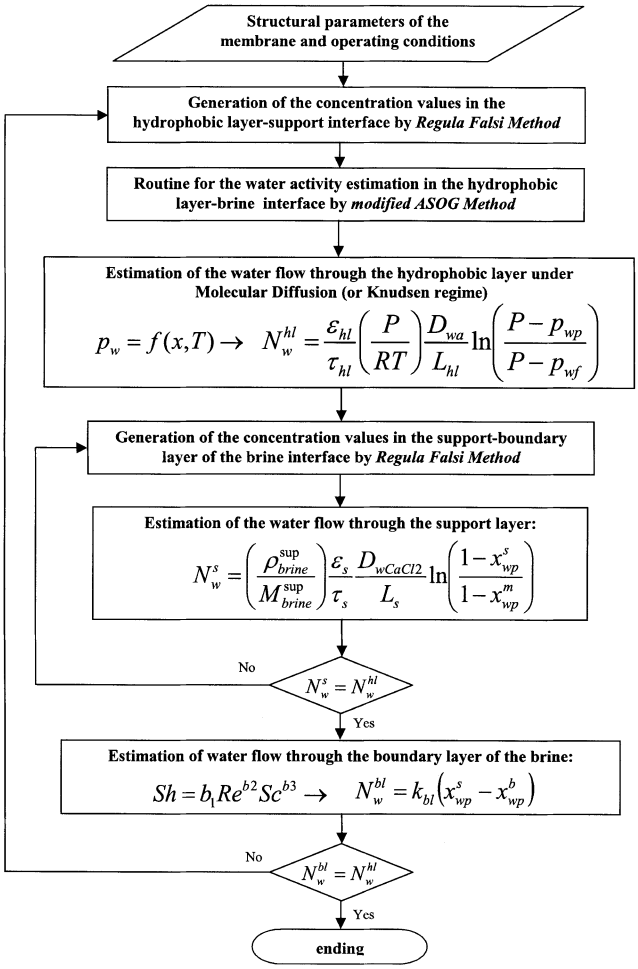

Figure 4. Algorithm for water-flow estimation at isothermal conditions when the mass transfer mechanism through the hydrophobic layer is the molecular diffusion.

Results and Discussion

Mass-transfer considerations

Courel and coworkers (Courel et al., 2000b) obtained very rapid water flows (between 1.6×10^{-3} and 3.4×10^{-3} kg·m^{-2}·s^{-1}). They explained that these results were a consequence of a specially designed membrane module configuration, which results in a complex but very efficient hydrodynamic flow pattern. Sheng and coworkers (Sheng et al., 1993) have also reported comparable water fluxes between 1.1×10^{-4} and 2.2×10^{-3} kg·m^{-2}·s^{-1} for a laboratory-scale module. Apart from these results, the water flows reported in the literature are generally much lower and below 1.1×10^{-3} kg·m^{-2}·s^{-1} (Bailey et al., 2000; Gostoli, 1999; Gabelman and Hwang, 1999).

The experimental setup used by Courel and coworkers (Courel et al., 2000a) was designed for flat-sheet membranes with a total surface area of 0.004 m^2. The membranes used by these authors (TF200 and TF450 from Pall Gelman) presented the same two-layer structure that was considered in the preceding section. The fluids were circulated cocurrently along both sides of the membrane, with an evenly distributed velocity profile and optimized circulation paths.

The developed program allows estimation of the water-flow values between 7.2×10^{-4} and 2.2×10^{-3} kg·m^{-2}·s^{-1} when the temperature lies between 290 and 305 K, the circulation rate of the brine varies between 0.5 and 4.5 m·s^{-1}, and the brine concentration is changed from 30 w/w % to 45 w/w % of $CaCl_2$. Under these conditions, the vapor flows calculated from Knudsen and molecular diffusion equations are nearly the same. Thus it is not possible to make a distinction between both transport regimes.

According to the manufacturer, the two membranes present different mean pore diameters: 0.2 μm for TF200 and 0.45 μm for TF450. In fact, it follows from a thorough investigation carried out directly on the two-layer structure by

Table 1. Parameters for Simulation with TF200 and TF450 Membranes

Parameter	Value
Hydrophobic Layer	PTFE
r_{hl}	4.5×10^{-8} m
L_{hl}	6.0×10^{-5} m
ϵ_{hl}	0.8
τ_{hl}	1.1
Support	Polypropylene
L_s	10.5×10^{-5} m
ϵ_s	0.6
τ_s	1.1

Source: Courel (1999).

Courel (Courel et al., 2001) that the structural properties of the two barriers are similar. These properties, which have been used for simulation purposes, are reported in Table 1.

The estimations were carried out applying two different approaches:

- A variation of the operating parameters according to experiments, where the water flow is calculated as a function of the salt concentration, circulation rate of the extraction brine, and the absolute temperature in the system.
- A variation of the resistance through the thickness of the gas film trapped in the hydrophobic layer.

The theoretical influence of the operating conditions or membrane structure on the OE process has been calculated and is given in Figures 5 and 6. Among the most interesting results of the simulation, Figure 5a shows the water-flow value estimated at isothermal conditions as a function of the circulation rate of the brine at different absolute temperatures. Obviously, the influence of the temperature is very important here. Under certain conditions, an increase of 10 K can produce a 40% enhancement on the water flow through the membrane.

Another key parameter is the brine concentration; its effect on the flux at different circulation rates can be observed in Figure 5b. From this figure we can conclude that the influence of concentration on mass transfer is more marked at the highest values of the circulation rate.

Figure 6 shows the result of the simulation carried out with membrane TF200, assuming that the gas-layer thickness within the membrane is 60 μm. It is worth recalling that this value corresponds to the PTFE-layer thickness. We can see that the calculated water flow values approach the experimental values obtained by Courel and coworkers, even if they are still underestimated.

The effect of the liquid penetration within the membrane structure can also be observed in the Figures 6. In fact, it generates a variation of the two resistances associated with the gas and liquid layers, respectively, trapped within the solid; thus it can affect the global-process performance. The simulation carried out at extreme liquid-penetration conditions, when the thickness of the gas layer is reduced to only 20 μm, provides an estimate that matches well the experimental data at a circulation rate below 1.5 $\mathrm{m\cdot s^{-1}}$.

From these results it also follows that, when the brine circulation rate is over 3 $\mathrm{m\cdot s^{-1}}$, the resistance of the boundary layer to mass transfer is not appreciable. Indeed, it is the only resistance that depends on hydrodynamics.

As a rule, it appears that the estimated water flow is always below the experimental one. Two facts could explain this result (Romero et al., 2001):

(1) One is the very complex geometry of the membrane module used by Courel (1999) in her experimental work. It is certainly responsible for a complex hydrodynamic behavior, which is difficult to take into account by means of a correlation as simple as the one selected [correlation of Calderbank and Young (Courel, 1999) for the turbulent flow regime, with $b_1 = 0.082$, $b_2 = 0.69$, and $b_3 = 0.33$; see Eq. 5)]. To check this fact, new experimental runs with a module presenting a simpler geometry and hydrodynamics are being developed.

(2) The second is the deeper penetration of water or of brine into the solid structure. In fact, the liquid penetration within the membrane is a function of the pressure of the circulating solutions. As explained earlier, the module presents a complex geometry, and the brine's increase in linear velocity could result in pressure enhancement, thus changing the extent of liquid penetration. The interactions between the membrane material, the brine, and the water also have to be considered. A possible surface modification of the hydrophobic membranes due to contact with the water and $CaCl_2$ solutions has been described by Barbe et al. (2000). The penetration of several liquids in this type of porous material has been quantified by Tröger (1998) for the determination of surface tension, and such a phenomenon needs to be considered.

Thermal effects in osmotic evaporation process: Simultaneous mass and heat transfer

As already explained the module used by Courel had a very complex geometry. In the absence of any appropriate correlation, all calculations were carried out using the value of a liquid heat-transfer coefficient that varies between 150 and 2,000 $\mathrm{W\cdot m^{-2}\cdot K^{-1}}$. The lower limit of 150 $\mathrm{W\cdot m^{-2}\cdot K^{-1}}$ (Welty et al., 1982) was considered to be the limit of maximum thermal polarization, whereas the upper value of 2,000 $\mathrm{W\cdot m^{-2}\cdot K^{-1}}$ was used taking the most favorable hydrodynamic conditions to heat transfer into consideration.

The effective thermal conductivities for each membrane layer have been calculated through Eqs. 13 and 15 and related to the thickness through Eqs. 12 and 14. Their values, k_{hl}^T for the hydrophobic layer and k_s^T for the wetted support, are equal to 0.072 $\mathrm{W\cdot m^{-1}\cdot K^{-1}}$ and 0.414 $\mathrm{W\cdot m^{-1}\cdot K^{-1}}$, respectively.

By comparing the results obtained at steady state, either considering the thermal effects or neglecting the temperature polarization, it appears that there is a decrease in the water-flow value of about 15% to 20% under the first hypothesis (see Table 2). We can observe that this decrease corresponds to a reduction of the driving force (that is, the difference of vapor pressure through the hydrophobic layer) caused by the temperature polarization. For all the simulations developed, the heat flux through the membrane remains less than 1200 $\mathrm{W\cdot m^{-2}}$.

The estimated concentration profiles are very similar no matter which method is used; heat transfer does not modify the results significantly (Table 2). The slight decrease in the

performance of the system due to the temperature polarization could be clearly explained by the strong relationship that exists between the temperature and the water-vapor pressure at saturation on the interfaces. Even if the temperature polarization is below 2.5 K, it is enough to produce an effect on the heat flow that obviously influences the water flow through the membrane. This dependence on temperature has been used for beneficial effects and motivated some authors to

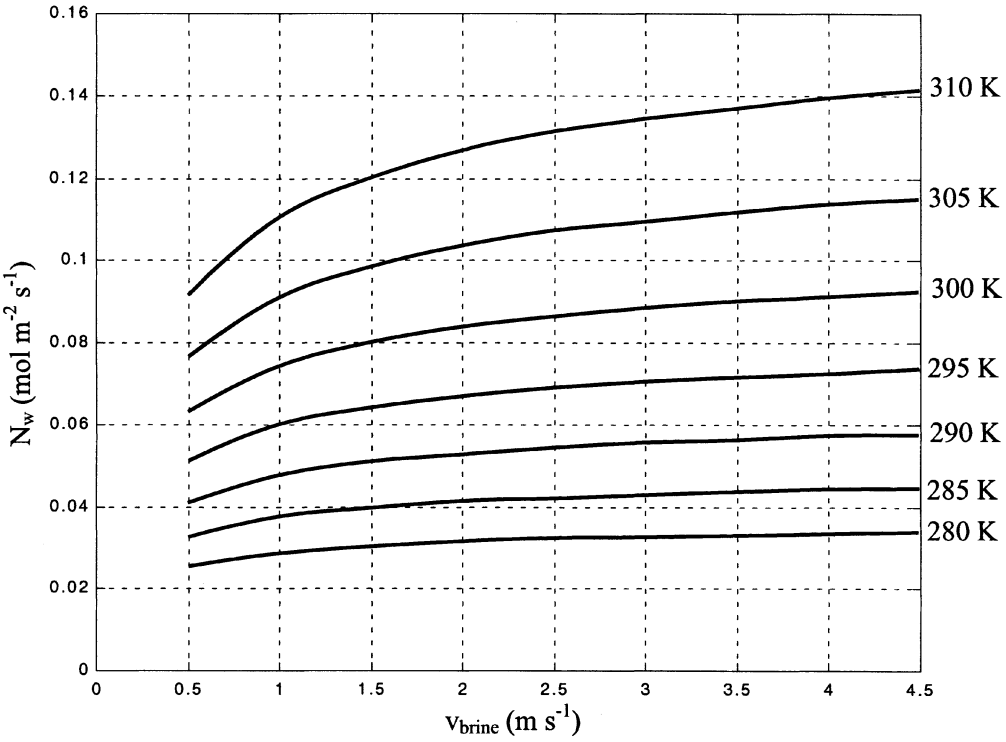

(a)

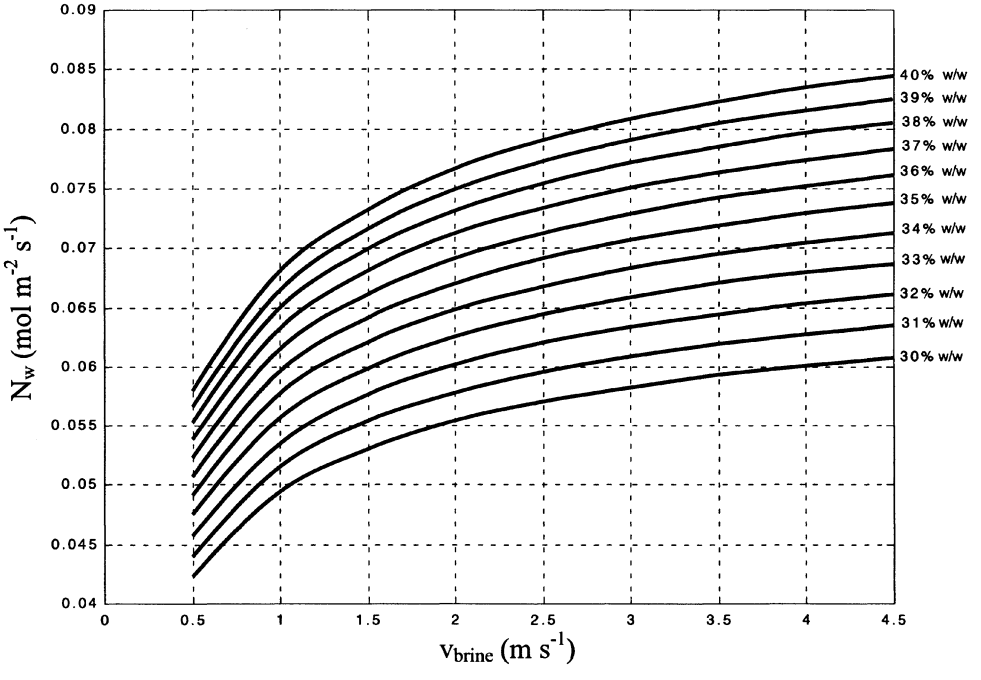

(b)

Figure 5. Water flow vs. brine circulation rate: (a) at different temperatures and brine concentration of 40% w/w; (b) at different brine concentrations and temperature of 298 K (hydrophobic layer in Knudsen diffusion).

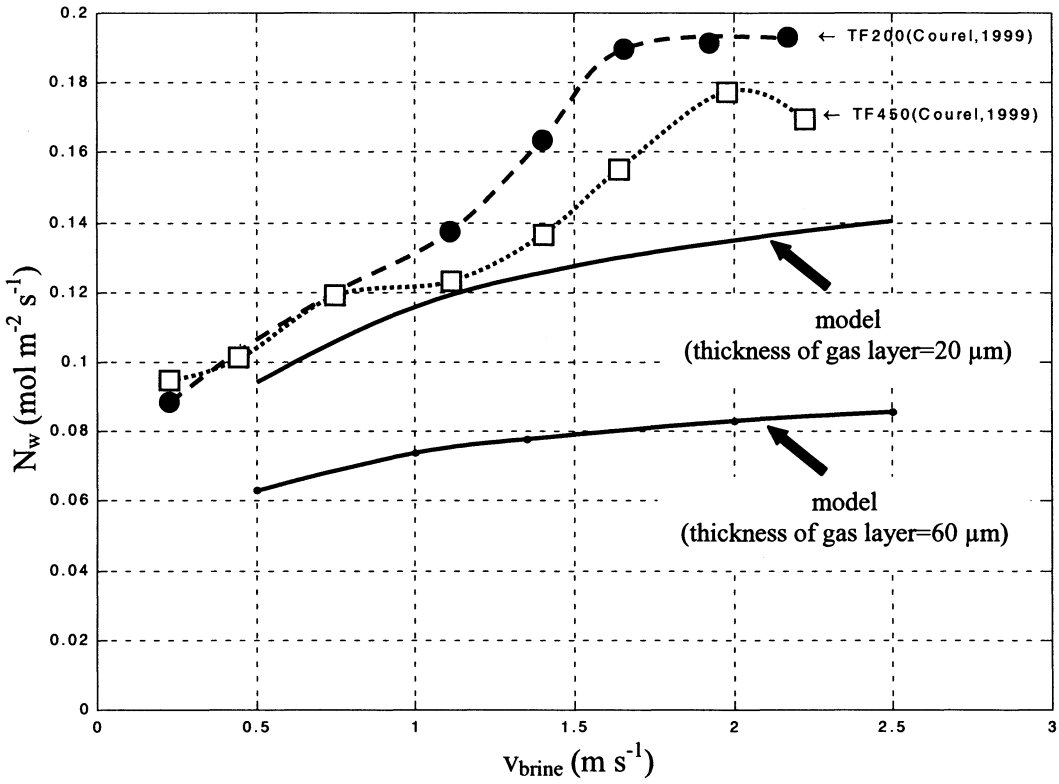

Figure 6. Water flow simulation vs. brine circulation rate at different values of gas layer thickness (hydrophobic layer in Knudsen diffusion), brine concentration of 45% w/w and $T = 298$ K.

carry out OE processes that combine the concentration and temperature gradients (Wang et al., 2001).

Vapor and liquid equilibrium in porous media

It is important to remember that the mass and heat fluxes are controlled by the transport conditions within each of the constituent layers of the system. In addition, the phase equilibrium that settles at each pore entrance introduces a complementary effective resistance. Some authors (Shin and Simandl, 1999) have considered that the estimation of this interface resistance, classically made by referring to what happens over a free liquid–vapor interface, could be erroneous due to the fact that the vapor–liquid equilibrium in heterogeneous media differs. This effect does not seem to affect significantly the estimates carried out with water, but it could generate larger deviations with mixtures of volatile compounds to be considered in future works (Shin and Simandl, 1999).

Conclusions

The results of simulation presented in this work make it possible to understand the behavior of the water flux reported in the literature for the osmotic evaporation process

Table 2. Simulation for Isothermal and Nonisothermal (Temperature Polarization) Conditions

Parameter or Variable	Est. Value Isothermal Cond.	Est. Value with Thermal Effects	Est. Value with Thermal Effects
Water flow through membrane (N_w)	0.0781 mol·m^{-2}·s^{-1}	0.0628 mol·m^{-2}·s^{-1}	0.0676 mol·m^{-2}·s^{-1}
Heat flow through membrane (Q)	0	159.7 W·m^{-2}	1,186.5 W·m^{-2}
Heat-transfer coeff. in feed solution (h_f)	∞	150 W·m^{-2}·K^{-1}	2,000 W·m^{-2}·K^{-1}
Heat-transfer coeff. in extraction brine (h_{brine})	∞	150 W·m^{-2}·K^{-1}	2,000 W·m^{-2}·K^{-1}
Heat-transfer coeff. of hydrophobic layer (h_{hl})	∞	1,198.5 W·m^{-2}·K^{-1}	1,198.5 W·m^{-2}·K^{-1}
Heat-transfer coeff. in wet support (h_s)	∞	3,938.1 W·m^{-2}·K^{-1}	3,938.1 W·m^{-2}·K^{-1}
Water-vapor pres. at solution–hydrophobic layer interface	3,142.10 Pa	2,947.90 Pa	3,032.55 Pa
Water-vapor pres. at hydrophobic layer–support interface	2,242.83 Pa	2,224.70 Pa	2,263.06 Pa
Temp. in solution to be treated (T_f^b)	298.00 K	298.00 K	298.00 K
Temp. on solution–hydrophobic layer interface (T_f^m)	298.00 K	296.94 K	297.41 K
Temp. on hydrophobic layer–support interface (T_p^m)	298.00 K	299.11 K	298.89 K
Temp. on solution–support–brine (T_p^s)	298.00 K	299.06 K	298.59 K
Salt conc. on hydrophobic layer–support interface	27.27 % w/w	29.78 % w/w	28.96 % w/w
Salt conc. on support–brine interface	32.57 % w/w	34.43 % w/w	33.82 % w/w

Membrane TF200, $v_{brine} = 1.35$ m·s^{-1}; $T_p^b = 298$ K; bulk salt concentration, 45% w/w $CaCl_2$.

(OE). In particular, in the case of the very high water-flux values obtained by Courel (1999) (0.15 $mol \cdot m^{-2} \cdot s^{-1}$, about 2.7 $10^{-3} \cdot kg \cdot m^{-2} \cdot s^{-1}$), they show well the general tendencies of evolution of performance as a function of operating variables and clearly indicate the main influence of the absolute temperature.

The OE process is mainly controlled by the driving force through the hydrophobic layer, that is, the difference in partial pressure of the water-vapor, which is not over 1000 Pa in the classic conditions found here.

The system is very sensitive to tangential flow conditions. A proper hydrodynamics characterization of the module, with appropriate correlations, is thus necessary to adequately compare the experimental and simulation results. The discrepancies observed in this work could be the result of complex module hydrodynamics that is not well described by the mathematical relations used, especially with respect to the liquid transfer coefficients. Regarding this aspect, new studies are in progress that involve simpler membrane geometry.

The liquid penetration in the membrane structure is a function of the pressure of the circulating solutions. It can significantly affect the performance of this technique, because it can generate important variations in the thickness of the different mass-transfer resistances that control the global mass-transport process.

Even if the temperature polarization does not affect the process strongly, it is advisable to attenuate its effect by using materials with high thermal conductivity values and well controlled hydrodynamics inside the membrane module.

The structure and modular design of this algorithm aim to generalize it to other membrane contact operations with separation such as membrane distillation, perstraction (Mulder, 1996; Gabelman and Hwang, 1999), or even reaction.

Acknowledgments

The financial support of the University of Santiago de Chile and the French Government for the Julio Romero's PhD studies is gratefully acknowledged.

Notation

b_1 = constant in Eq. 5
b_2 = constant in Eq. 5
b_3 = constant in Eq. 5
D = diffusion coefficient, $m^2 \cdot s^{-1}$
G = permeance, $mol \cdot m^{-2} \cdot s^{-1} \cdot Pa^{-1}$
h = heat-transfer coefficient, $J \cdot s^{-1} \cdot m^{-2} \cdot K^{-1}$
k = mass-transfer coefficient, $mol \cdot m^{-2} \cdot s^{-1}$
k^T = thermal conductivity, $J \cdot s^{-1} \cdot m^{-1} \cdot K^{-1}$
L = thickness, m
M = molecular weight, $kg \cdot mol^{-1}$
N = mass flow, $mol \cdot m^{-2} \cdot s^{-1}$
P = pressure in the pore of the hydrophobic membrane, Pa
p = partial pressure, Pa
Q = transmembrane heat flow, $J \cdot s^{-1} \cdot m^{-2}$
R = gas constant, $J \cdot mol^{-1} \cdot K^{-1}$
r = pore radius, m
Re = Reynolds number
Sc = Schmidt number
Sh = Sherwood number
T = temperature, K
x = water molar fraction in liquid phase
y = water molar fraction in gas phase

Greek letters

γ = activity coefficient
ΔH = latent heat, $J \cdot mol^{-1}$
ϵ = porosity
ρ = density, $kg \cdot mol^{-3}$
τ = tortuosity

Subscripts and superscripts

a = air
bl = boundary layer
brine = brine
$CaCl_2$ = calcium chloride
MD = molecular-diffusion regime
f = feed solution
gas = gas phase within the pores
hl = hydrophobic layer
i = i-component
Kn = Knudsen regime
p = permeate side
polymer = polymer property
s = support property
v = vaporization
w = water
I = first layer: boundary layer in the feed solution
II = second layer: hydrophobic layer in the membrane
III = third layer: penetrated support
IV = fourth layer: boundary layer in the brine
b = bulk conditions
C = combinatorial
$D\text{-}H$ = Debye–Hückel
m = in contact with the hydrophobic layer
R = residual
s = in contact with the support
sup = at average conditions within the support

Literature Cited

Bailey, A. F. G., A. M. Barbe, P. A. Hogan, R. A. Johnson, and J. Sheng, "The Effect of the Ultrafiltration on the Subsequent Concentration of Grape Juice by Osmotic Distillation," *J. Memb. Sci.*, **164**, 195 (2000).

Bandini, S., A. Saavedra, and G. C. Sarti, "Vacuum Membrane Distillation: Experiments and Modelling," *AIChE J.*, **43**, 398 (1997).

Barbe, A. M., P. A. Hogan, and R. A. Johnson, "Surface Morphology Changes During Initial Usage of Hydrophobic, Microporous Polypropylene Membranes," *J. Memb. Sci.*, **172**, 149 (2000).

Correa, A., J. F. Comesaña, J. M. Correa, and A. M. Sereno, "Measurement and Prediction of Water Activity in Electrolyte Solutions by a Modified ASOG Group Contribution Method," *Fluid Phase Equilib.*, **129**, 267 (1997).

Courel, M., *Etude des Transferts de Matière en Évaporation Osmotique: Application à la Concentration des Jus de Fruits*, PhD Thesis, Univ. of Montpellier II, Montpellier, France (1999).

Courel, M., M. Dornier, J. M. Herry, G. M. Rios, and M. Reynes, "Effect of Operating Conditions on Water Transport During the Concentration of Sucrose Solutions by Osmotic Distillation," *J. Memb. Sci.*, **170**, 281 (2000a).

Courel, M., M. Dornier, G. M. Rios, and M. Reynes, "Modelling of Water Transport in Osmotic Distillation Using Asymmetric Membrane," *J. Memb. Sci.*, **173**, 107 (2000b).

Courel, M., E. Tronel-Peyroz, G. M. Rios, M. Dornier, and M. Reynes, "The Problem of Membrane Characterisation for the Process of Osmotic Evaporation," *Desalination*, **140**, 15 (2001).

Deblay, P., "Un Nouveau Procédé de Concentration de Solutions Aqueuses: l'Évaporation Osmotique," *BIOS*, **250**, 56 (1994).

Gabelman, A., and S. Hwang, "Hollow Fiber Membranes Contactors," *J. Memb. Sci.*, **159**, 61 (1999).

Godino, P., L. Peña, and J. I. Mengual, "Membrane Distillation: Theory and Experiments," *J. Memb. Sci.*, **121**, 83 (1996).

Gostoli, C., "Thermal Effects in Osmotic Distillation," *J. Memb. Sci.*, **163**, 75 (1999).

Iversen, S. B., V. K. Bhatia, K. Dam-Johansen, and G. Jonsson, "Characterization of Microporous Membranes for Use in Membrane Contactors," *J. Memb. Sci.*, **130**, 205 (1997).

Keryszig, E., *Matemáticas Avanzadas para Ingeniería*, Limusa–Noriega Editores, Mexico City, México (1991).

Kunz, W., A. Benhabiles, and R. Ben-Aïm, "Osmotic Evaporation Through Macroporous Hydrophobic Membranes: A Survey of Current Research and Applications," *J. Memb. Sci.*, **121**, 25 (1996).
Lawson, K. W., and D. R. Lloyd, "Membrane Distillation (review)," *J. Memb. Sci.*, **124**, 1 (1997).
Lefebvre, M. S., R. A. Johnson, and V. Yip, "Theoretical and Practical Aspects of Osmotic Distillation," *Proc. Int. Cong. Membrane Processes*, Tokyo, Japan, p. 55 (1987).
Mokhtari, M., *Matlab* 5.2 & 5.3 *et Simulink* 2 & 3 *pour Étudiants et Ingénieurs*, Springer-Verlag, Berlin (2000).
Mulder, M., *Basic Principles of Membrane Technology*, Kluwer, Dordrecht, The Netherlands (1996).
Peña, L., M. P. Godino, and J. I. Mengual, "A Method to Evaluate the Net Membrane Distillation Coefficient," *J. Memb. Sci.*, **143**, 219 (1998).
Quarteroni, A., *Méthodes Numériques pour le Calcul Scientifique*, Springer-Verlag, Paris (2000).
Romero, J., G. M. Rios, J. Sanchez, and A. Saavedra, "Modelling and Simulation of Osmotic Evaporation Process," *Proc. Conf. Engineering with Membranes*, Vol. II, Granada, p. 297 (2001).
Sheng, J., "Osmotic Distillation Technology and Its Applications," *Aust. Chem. Eng. Conf.*, **3**, 429 (1993).
Shin, Y., and J. Simandl, "Vapor and Liquid Equilibria in Porous Media," *Fluid Phase Equilib.*, **166**, 79 (1999).
Tröger, J., K. Lunkwitz, K. Grundke, and W. Bürger, "Determination of the Surface Tension of Microporous Membranes Using Wetting Kinetics Measurements," *Colloids Surf. A: Physicochem. Eng. Aspects*, **134**, 299 (1998).
Wang, Z., F. Zheng, and S. Wang, "Experimental Study of Membrane Distillation with Brine Circulated in the Cold Side," *J. Memb. Sci.*, **183**, 171 (2001).
Welty, J. R., C. E. Wicks, and R. E. Wilson, *Fundamentos de Transferencia de Momento Calor y Masa*, Limusa–Noriega Editores, Mexico City, México (1982).

Manuscript received Oct. 12, 2001, and revision received July 3, 2002.